Probabilistic Reachability Analysis of the Tap Withdrawal Circuit in Caenorhabditis elegans

Md. Ariful Islam*, Qinsi Wang*, Ramin M. Hasani**, Ondrej Balún**,
Edmund M. Clarke*, Radu Grosu** Scott A. Smolka†
* Deparment of Computer Science, Carnegie Mellon University
{mdarifui, qinsiw, emc}@cs.cmu.edu
†Department of Computer Science, Stony Brook University
{sas}@cs.stonybrook.edu
**Department of Informatics, Vienna University of Technology
{ramin.hasani, radu.grosu}@tuwien.ac.at
ondrejbalun@gmail.com

Abstract—We present a probabilistic reachability analysis of a (nonlinear ODE) model of a neural circuit in *Caeorhabditis elegans* (C. elegans), the common roundworm. In particular, we consider *Tap Withdrawal* (TW), a reflexive behavior exhibited by a C. elegans worm in response to vibrating the surface on which it is moving. The neural circuit underlying this response is the subject of this investigation. Specially, we perform bounded-time reachability analysis on the TW circuit model of Wicks et al. (1996) to estimate the probability of various TW responses. The Wicks et al. model has a number of parameters, and we demonstrate that the various TW responses and their probability of occurrence in a population of worms can be viewed as a problem of *parameter uncertainty*.

Our approach to this problem rests on encoding each TW response as a hybrid automaton with parametric uncertainty. We then perform probabilistic reachability analysis on these automata using a technique that combines a δ-decision procedure with statistical tests. The results we obtain are a significant extension of those of Wicks et al. (1996), who equip their model with fixed parameter values that reproduce a single TW response. In contrast, our technique allow us to more thoroughly explore the models parameter space using statistical sampling theory, identifying in the process the distribution of TW responses.

Wicks et al. conducted a number of *ablation experiments* on a population of worms in which one or more of the neurons in the TW circuit are surgically ablated (removed). We show that our technique can be used to correctly estimate TW response-probabilities for four of these ablation groups. We also use our technique to *predict* TW response behavior for two ablation groups not previously considered by Wicks et al.

I. INTRODUCTION

Due to the simplicity of its nervous system (302 neurons, ~5,000 synapses) and the breadth of research on the animal, *C. elegans*, the common roundworm, is a model system for neuroscience. The complete connectome of the worm is documented [1], [2], and a number of interesting experiments have been carried out on its locomotory neural circuits connecting sensory neurons to motor neurons [3], [4], [5], [6].

We are particularly interested in the *Tap Withdrawal* (TW) neuronal circuit, which governs the reactionary motion of the animal when the petri dish in which it swims is subjected to a mechanical tap [7]. (A related circuit, *touch sensitivity*, controls the reaction of the worm when a stimulus is applied to a single point on the body.)

The term "tap withdrawal" refers to the fact that worms swimming in a petri dish tend to *withdraw* (turn around and swim in the opposite direction) when subjected to a tap stimulus. Presumably, this is because the tap causes them to sense danger in their surrounding environment. The worms, however, can be conditioned or *habituated* to ignore this stimulus [8].

Studies of the TW circuit have traditionally involved using lasers to ablate different neurons in the circuit of multiple animals, and then measuring the response behavior when tap stimuli are applied [9]. Such is the case for [10]; see also Fig. 1. Such behaviors are logged with the percentage of the experimental population to display that behavior.

Moreover, with the aim of predicting synaptic polarities (unknown parameters) of the TW circuit, the dynamics of the membrane potential of different neurons has been mathematically modeled [11]. This model is in the form of a system of nonlinear ODEs with an indication of the polarity (inhibitory or excitatory) of each neuron in the circuit.

The Wicks et al. circuit model has a significant number of parameters, including gap-junction conductance, membrane capacitance and leakage current, that decisively affect the circuit's behavior. Fixed values for these parameters have been provided based on the measurements performed on single in-vitro neurons [11]. The model therefore produces the predominant behavior in most ablation groups with a few exceptions.

While the experimental work and the model presented in [11] were by no means insubstantial, the exploration of the model is vastly incomplete. Fixed parameter values fit through experimentation cause the model to replicate the predominant behavior seen in the mentioned experiments, but little can be gained beyond that. All such animals are not created equal owing to genetic variation, and, during their lifetime, they are exposed to stimuli of varying intensity, duration,

and frequency. Carefully and (semi-)exhaustively varying the circuit parameters of the [11] model should provide us with insights underlying these processes, and ultimately help us to understand the learning process in neural circuits.

Towards this end, in [12], we explored the parameter spaces of the Wicks et al. model using reachability analysis to estimate key model parameters for various TW responses. The main idea was to augment the state space of the model with parameters and compute "reachtubes" (overapproximation of the model's reachable state space) by varying parameters in the initial conditions. We performed our reachability analysis based on automatically computing discrepancy functions developed by Fan et al. [13].

To cover the parameter space of interest, the technique in [13] divides the space into a finite number of δ-balls. The required number of δ-balls depends on the maximum eigenvalue of the Jacobian of the dynamics. If the maximum eigenvalue is positive, the computed reachtube may blow up so much that the property can not be verified. In such case, the technique refines the δ-ball with smaller balls and redo the computation for all of them. Additionally, the required number of δ-balls increases exponentially over the number of variables in the model.

As, in the Wicks et al. model, the number of parameters is 27, the augmented system, along with 9 state variables, will have 36 state variables in total. For this model, the maximum eigenvalue is also not always negative over time. Thus, the technique in [13], simply does not scale up to explore the complete parameter-space of the model.

For this reason, in [12], we augmented the model with at most three parameters. Despite considering a small number of parameters, we still could not cover the entire biologically relevant range for these parameters. We were able to explore only a tiny fraction of the parameter space.

In this paper, we address the same problem, but using the more robust technique of statistical sampling theory. We perform bounded-time probabilistic reachability analysis on the Wicks et al. model to estimate the probability of various TW responses related to parameter uncertainty. Instead of providing a certain answer about a reachability problem of a dynamical system, this analysis provides an estimated probability. We take advantage of this probabilistic analysis to derive population percentages that exhibit various behaviors in response to tap stimuli. Importantly, statistical sampling theory combined with reachability analysis can handle large-scale systems for which traditional reachability analysis may not scale.

For the purpose of our analysis, we first encode various responses of the TW circuit as stochastic hybrid automata. We then perform the probabilistic reachability analysis to estimate the probability for each response of the TW circuit using the SReach tool [14], which is a probabilistic bounded reachability analyzer. This technique allows us to augment the model with a large number of parameters and to more thoroughly explore the models parameter space using statistical sampling theory, identifying in the process the distribution of TW responses.

The rest of the paper is organized as follows. Section II introduces the TW circuit and the Wicks et al. model. Sections III enumerates all response patterns of the TW circuit. Section IV

describes how we formulate probabilistic reachability analysis of TW circuit using SReach. Section V presents our results for various ablation groups. Section VI considers related work. Section VII offers our concluding remarks and directions for future work.
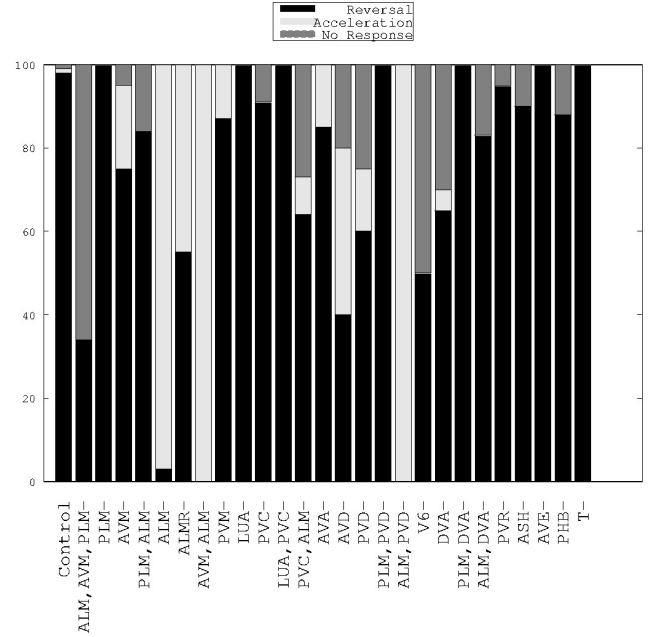

Fig. 1: Effect of ablation on Tap Withdrawal reflex (experimental results). The length of the bars indicate the fraction of the population demonstrating the particular behavior. [10]

II. BACKGROUND

In *C. elegans*, there are three classes of neurons: *sensory*, *inter*, and *motor*. For the TW circuit, the sensory neurons are *PLM*, *PVD*, *ALM*, and *AVM*, and the inter-neurons are *AVD*, *DVA*, *PVC*, *AVA*, and *AVB*. The model we are using abstracts away the motor neurons as simply forward and reverse movement. Neurons are connected in two ways: electrically via bi-
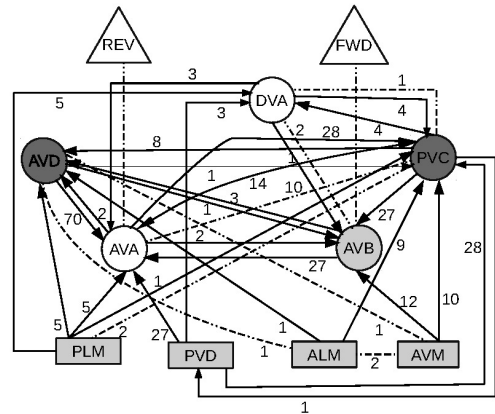

Fig. 2: Tap Withdrawal Circuit of C. elegans. Rectangle: Sensory Neurons; Circle: Inter-neurons; Dashed Undirected Edge: Gap Junction; Solid Directed Edge: Chemical Synapse; Edge Label: Number of Connections [15]; Dark Gray: Excitatory Neuron; Light Gray: Inhibitory Neuron; White: Unknown Polarity. FWD: Forward Motor system; REV: Reverse Motor System.

directional *gap junctions*, and chemically via uni-directional chemical *synapses*. Each connection has varying degrees of throughput, and each neuron can be *excitatory* or *inhibitory*, governing the polarity of transmitted signals. These polarities were experimentally determined in [11], and used to produce the circuit shown in Fig. 2.

In [10], Wicks et al. performed a series of laser ablation experiments in which they knocked out neurons in a group of animals (worms), subjected them to a tapped surface, and recorded the magnitude and direction of the resulting behavior. Fig. 2 shows the response types for each of their experiments.

A. Mathematical Model of the TW Circuit

The dynamics of a neuron's membrane potential, *V*, is determined by the internal state of the neuron together with sum of all input currents [16], written as:

$$\frac{dV}{dt} = \frac{1}{CR}(V^{leak} - V) + \frac{1}{C}\sum (I^{gap} + I^{syn} + I^{stim})$$

where *V* represents the *membrane potential*, *C* is the *membrane capacitance*, *R* is the *membrane resistance*, V^{leak} is the *leakage potential*, I^{gap} and I^{syn} are gap-junction and the chemical synapse currents, respectively, and I^{stim} is the applied external *stimulus* current. The summations are over all neurons with which this neuron has a (gap-junction or synaptic) connection.

The current flows between neuron *i* and *j* via n_{ij} gap-junctions can be seen as the current passing through *n* parallel resistors. Therefore, based on the Ohm's law, one can derive the gap-junction current equation as follows:

$$I_{ij}^{gap} = n_{ij}g_m^{gap}(V_j - V_i)$$

where the constant g_m^{gap} is the *maximum conductance* of the gap junction, and n_{ij} is the number of gap-junctions between neurons *i* and *j*. The conductance g_m^{gap} defines the strength of a connection between two neurons. As a consequence, it sets the amount of shared information of the two neurons. This key parameter significantly affects the behavior of the neural circuits.

Chemical synapses transfer information by releasing neurotransmitters [17]. Inspired by Hodgkin-Huxley model of ionic channels [18], one can model such behavior as a synaptic current flowing from presynaptic neuron *j* to post-synaptic neuron *i* as below:

$$I_{ij}^{syn} = n_{ij}^{syn}g_{ij}^{syn}(t)(E_j - V_i)$$

where $g_{ij}^{syn}(t)$ is the voltage-dependent synaptic conductance of neuron *i*, n_{ij}^{syn} is the number of synaptic connections from neuron *j* to neuron *i*, and E_j is the *reversal potential* of neuron *j* for the synaptic conductance.

The chemical synapse is characterized by a synaptic sign, or polarity, specifying if said synapse is excitatory or inhibitory. The value of E_j is assumed to be constant for the same synaptic sign.

For a neuron of C. elegans at equilibrium, the membrane potential on average is around -30mV. According to the Eq. II-A, by setting the reversal potential value to a higher values than the resting potential of a neuron, the synaptic current increases and therefore an excitatory behavior is realized. On the contrary, an inhibitory synapse is developed by placing the value of the reversal potential less than the equilibrium potential of the neuron.

Dynamics of the Synaptic conductance depends on the membrane potential state of the presynaptic neuron V_j. For the sake of simplicity, Wicks et al. model such dynamics by the steady-state response of the synapse as follows

$$g_{ij}^{syn}(t) = g_\infty^{syn}(V_j)$$

where the conductance at steady-state is given by:

$$g_\infty^{syn}(V_j) = \frac{g_m^{syn}}{1 + \exp{(k\frac{V_j - V_j^{eq}}{V_{Range}})}}$$

g_m^{syn} presents the *maximum synaptic conductance*, V_j^{eq} is the *pre-synaptic equilibrium potential*, and V_{Range} is the *pre-synaptic voltage range* over which the synapse is activated. *k* is an experimentally derived constant, valued at -4.3944.

Combining all of the above pieces, the mathematical model of the TW circuit is a system of nonlinear ODEs, with each state variable defined as the membrane potential of a neuron in the neural circuit. Consider a circuit with *N* neurons. The dynamics of the ith neuron of the circuit is given by:

$$\frac{dV_i}{dt} = \frac{V_{l_i} - V_i}{C_iR_i} + \sum_{j=1}^{N}(I_{ij}^{gap} + I_{ij}^{syn} + I_i^{stim}) \qquad (1)$$

$$I_{ij}^{gap} = n_{ij}^{gap}g_m^{gap}(V_j - V_i) \qquad (2)$$

$$I_{ij}^{syn} = n_{ij}^{syn}g_{ij}^{syn}(E_j - V_i) \qquad (3)$$

$$g_{ij}^{syn} = \frac{g_m^{syn}}{1 + \exp{(k\frac{V_j - V_j^{eq}}{V_{Range}})}}. \qquad (4)$$

The equilibrium potentials (V^{eq}) of the neurons are computed by setting the left-hand side of Eq. (1) to zero [11]. This leads to a system of linear equations, that can be solved as follows:

$$V^{eq} = A^{-1}b \qquad (5)$$

where matrix *A* is given by:

$$A_{ij} = \begin{cases} -R_i n_{ij}^{gap}g_m^{gap} & \text{if } i \neq j \\ 1 + R_i\sum_{j=1}^{N} n_{ij}^{gap}g_{ij}^{gap}g_m^{syn}/2 & \text{if } i = j \end{cases}$$

and vector *b* is written as:

$$b_i = V_{l_i} + R_{m_i}\sum_{j=1}^{N} E_j n_{ij}^{syn}g_m^{syn}/2.$$

III. TAP WITHDRAWAL RESPONSE PATTERNS

The Wicks et al. model does not explicitly incorporate nematode locomotion. It simply defines the relationship between the animals locomotion and activation of the TW circuit that controls the behavior.

Wicks et al. assumes that the output of the TW circuit controls locomotory behavior primarily through the action of the inter-neurons AVB and AVA. The AVA interneurons make gap junctions and chemical synapses with motor neurons AS,

VA, and DA that excite backward locomotion, whereas the AVB interneurons form gap junctions with the motor neurons VB and DB that excite forward locomotion. Thus, Wicks et al. simply assume that the degree of backward (forward) locomotion is proportional to the depolarization of the AVA (AVB) interneuron and inversely proportional to the depolarization of the AVB (AVA) interneuron. Recently, Kawano et al. present
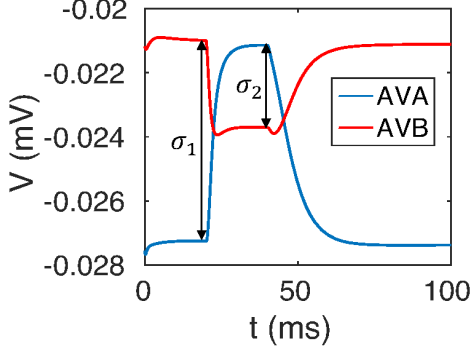

Fig. 3: Illustration of σ_1 and σ_2.

a study in [19] that supports the assumptions made by Wicks et al. on directional movement of C. elegans. Through in-vivo calcium imaging, electrophysiology and behavioral analyses of wild-type animals and innexin mutants, they show that the initiation of reversal movement is directly correlated with a increased calcium level in AVA. In contrast, the initiation of forward movement is associated with an increased calcium level in AVB and a decrease of the calcium transient correlated with either a reduced forward velocity or reversals.

Under standard laboratory culture conditions, the animal predominantly generates continuous forward movement without any tap stimulation [20], [21]. In [10], Wicks et al. experienced, through in vivo experiment, only three tap withdrawal responses: reversal, acceleration and no response. The simulation of the Wicks et al. model for certain ablation group (e.g., AVM,PVC- ablation group), however, shows the animal can also predominantly generate continuous backward movement without any tap stimulation. Additionally, the study of Kawano et al. supports the evidence of new type of response like deceleration (reduced forward velocity). These lead us to believe that, at least in theory, it is possible to have few more tap withdrawal responses as compared to what Wicks et al. experienced in their wet-lab experiments.

Similar to [11], [19], we consider the directional movement can be inferred based on the voltage difference between AVA and AVB interneurons:

- Forward movement: $v_{AVB} > v_{AVA}$

- Backward movement: $v_{AVB} < v_{AVA}$

- No movement: $v_{AVB} \sim v_{AVA}$

Assume that $\sigma_i = v_{AVB}^i - v_{AVA}^i$, $i \in \{1, 2\}$ be the voltage differences between AVB and AVA interneurons during non-stimulation and stimulation period, respectively, as shown in Fig. 3 and ϵ is some small positive number. Based σ_1, we categorize the TW responses into two subgroups:

- When $\sigma_1 >= 0$:
  1) Reversal: $\sigma_2 <= -\epsilon$
  2) No response: $|\sigma_2| <= \epsilon$
  3) Forward acceleration: $(\sigma_2 >= \epsilon) \wedge (\sigma_2 >= \sigma_1)$
  4) Forward deceleration: $(\sigma_2 >= \epsilon) \wedge (\sigma_2 < \sigma_1)$

- When $\sigma_1 < 0$:
  1) Forward: $\sigma_2 >= \epsilon$
  2) No response: $|\sigma_2| <= \epsilon$
  3) Backward acceleration: $(\sigma_2 <= -\epsilon) \wedge (\sigma_2 <= \sigma_1)$
  4) Backward deceleration: $(\sigma_2 >= \epsilon) \wedge (\sigma_2 > \sigma_1)$

Fig. 4 shows all four response patterns for the first subgroup. The response patterns for the second subgroup, however, will have the similar structures, if we interchange AVB with AVA in the figure.

IV. Probabilistic Reachability Analysis of TW Circuit

In this section, we present a bounded-time probabilistic reachability analysis to estimate the probability of various TW responses, caused due to parameter uncertainty. Our approach to this problem rests on encoding each TW response as a hybrid automaton with parametric uncertainty. We then apply probabilistic reachability analysis on each automaton that combines δ decision procedure with statistical tests.

Probabilistic reachability analysis using SReach:

SReach [14] is a probabilistic bounded reachability analyzer for two classes of models of stochastic hybrid systems: (nonlinear) hybrid automata with parametric uncertainty, and probabilistic hybrid automata with additional randomness. It takes a stochastic hybrid automaton $\mathcal{H}_s$, reachability properties $\mathcal{P}$, a numerical error bound $\delta \in \mathbb{Q}^+$, an unrolling depth $k \in \mathbb{N}$, and a chosen statistical testing method as inputs. It then encodes uncertainties in the given stochastic hybrid automaton $\mathcal{H}_s$ using random variables, and samples them according to the given distributions. For each sample, a corresponding intermediate HA is generated by replacing random variables with their assigned values. Then, the δ-complete analyzer *dReach* [22] is utilized to analyze each intermediate HA M_i, together with the desired precision δ and unfolding depth k. The analyzer returns either unsat or δ-sat for M_i. This information is then used by a chosen statistical testing procedure to decide whether to stop or to repeat the procedure, and to return the estimated probability.

SReach supports a number of hypothesis testing and statistical estimation techniques (see [14] for details). All methods produce answers that are correct up to a precision that can be set arbitrarily by the user. SReach can answer two types of questions:

- With hypothesis testing methods, SReach can answer qualitative questions, such as "Does the model satisfy a given reachability property in k steps with probability greater than a certain threshold?"

- With statistical estimation techniques, SReach can offer answers to quantitative problems. For instance,
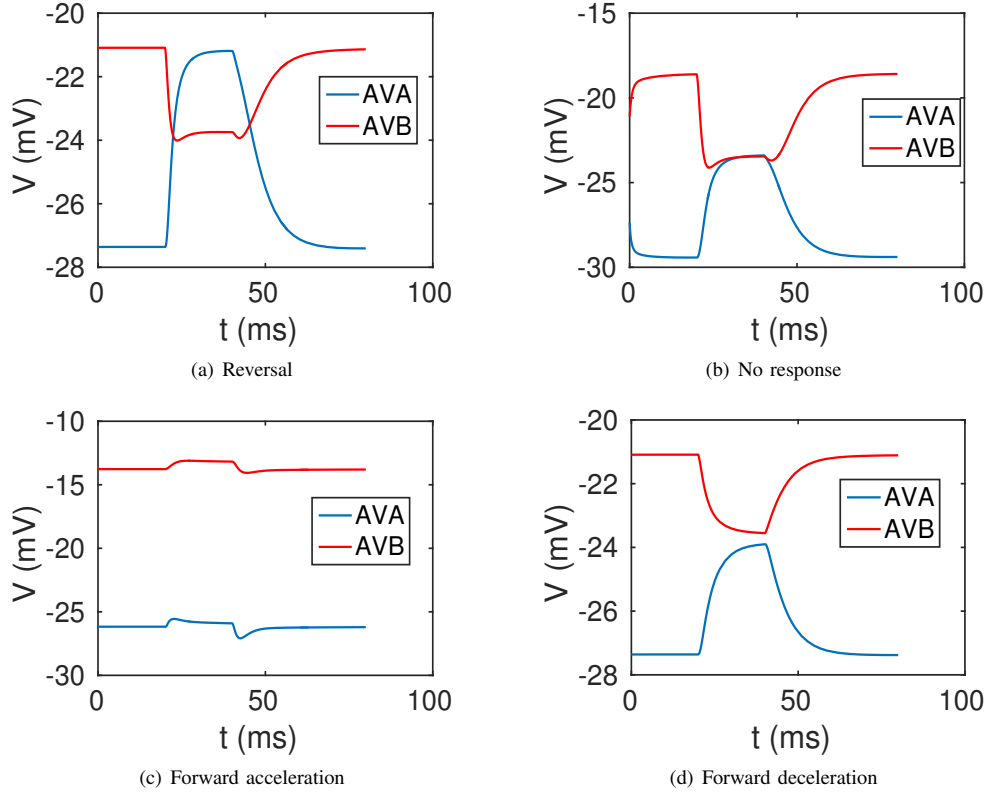
(a) Reversal

(b) No response

(c) Forward acceleration

(d) Forward deceleration

Fig. 4: Different tap withdrawal responses when, before the applying tap stimulation, the animal moves in forward direction.

"What is the probability that the model satisfies a given reachability property in k steps?"

SReach can also handle additional types of interesting problems, including the *model validation/falsification* problem with prior knowledge, the *parameter synthesis* problem, and the *sensitivity analysis*, by encoding them as bounded reachability problems.

Normalization of the Wicks et al. model

SReach internally uses dReach [23], which relies on numerical computation. As the the values of the parameters in the Wicks et al. model are in the order of 10^{-9} to 10^{-12}, the computation often suffers from numerical instability. To take into account this issue, we normalize the Wicks et al. model with respect to the capacitance, which is a common practice in modeling biological systems [24]. The values of the parameter in this normalized model are in the order of 10 to 10^3.

To normalize, we combine Eqs.(1) to (4):

$$\dot{V}_i = \frac{V_{l_i} - V_i}{R_i C_i} + \frac{g_m^{gap}}{C_i} \sum_{j=1}^{N} n_{ij}^{gap}(V_j - V_i)$$
$$+ \frac{g_m^{syn}}{C_i} \sum_{j=1}^{N} \frac{n_{ij}^{syn}(E_j - V_i)}{1 + \exp\left(k\frac{V_j - V_j^{EQ}}{V_{Range}}\right)} + \frac{1}{C_i} I_i^{stim}$$

Now letting $g_i^{leak} = \frac{1}{R_i C_i}$, $g_i^{gap} = \frac{g_m^{gap}}{C_i}$, $g_i^{syn} = \frac{g_m^{syn}}{C_i}$ and $I_i^{ext} = \frac{I_i^{stim}}{C_i}$ the normalized system dynamics can be written as:

$$\dot{V}_i = g_i^{leak}(V_{l_i} - V_i) + g_i^{gap} \sum_{j=1}^{N} n_{ij}^{gap}(V_j - V_i)$$
$$+ g_i^{syn} \sum_{j=1}^{N} \frac{n_{ij}^{syn}(E_j - V_i)}{1 + \exp\left(k\frac{V_j - V_j^{eq}}{V_{Range}}\right)} + I_i^{ext} \quad (6)$$

Hybrid automaton for TW circuit M_{TW}:

For the TW circuit, Wicks et al. model the tap stimulus as a phasic current that is applied to sensory neurons (AVM, ALM and PLM) simultaneously. The phasic current is, typically, a square-wave signal with a fixed duration. Due to the piecewise continuous nature of this signal, we represent Wicks et al. model as a hybrid automaton by dividing the dynamics into stimulus and non-stimulus modes. Additionally, when a tap is applied to the worm, it is assumed that the worm is operating in a stable condition. To take this into account, we apply the stimulation after a transition period. Assume that $[0, \tau_i]$ is the transition period, $[\tau_i, \tau_f]$ is the stimulation period and $[0, \tau_s]$ is the total simulation duration. Fig. 5 shows the hybrid automaton M_{TW} for the Wicks et al. model. The subscript i and j in the figure are used to denote the sensory neurons and the interneurons, respectively. We add an additional variable τ to support time-triggered jump from one mode to another.
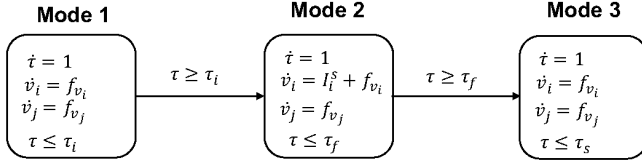
Mode 1
$$\dot{t} = 1$$
$$\dot{v}_i = f_{v_i}$$
$$\dot{v}_j = f_{v_j}$$
$$\tau \le \tau_i$$

$\tau \ge \tau_i$

Mode 2
$$\dot{t} = 1$$
$$\dot{v}_i = I_i^s + f_{v_i}$$
$$\dot{v}_j = f_{v_j}$$
$$\tau \le \tau_f$$

$\tau \ge \tau_f$

Mode 3
$$\dot{t} = 1$$
$$\dot{v}_i = f_{v_i}$$
$$\dot{v}_j = f_{v_j}$$
$$\tau \le \tau_s$$

Fig. 5: The 3-mode hybrid automaton M_{TW} for the Wicks et al. model

TW response as Hybrid Automaton, M_ϕ:

In section 3, we enumerated all possible TW responses and formalized them in terms of σ_1 and σ_2, the steady-state voltage difference between AVB and AVA interneurons during non-stimulus and stimulation period. Hence, to encode a TW response ϕ as hybrid automaton M_ϕ, we augment M_{TW} by adding two additional state variables σ_1 and σ_2. As these two variables measure the steady-state voltage differences, which are constant in time, the vector-fields for them are set to zero. However, as shown in Fig. 6, both σ_1 and σ_2 are reset to $v_{AVB} - v_{AVA}$ during the jump from "Mode 1" to "Mode 2" and "Mode 2" to "Mode 3", respectively. This ensures the correct values of σ_1 and σ_2 in "Mode 3".

Mode 1
$$\dot{t} = 1$$
$$\dot{v}_i = f_{v_i}$$
$$\dot{v}_j = f_{v_j}$$
$$\dot{\sigma}_1 = 0$$
$$\dot{\sigma}_2 = 0$$
$$\tau \le \tau_i$$

$\tau \ge \tau_i$

$\sigma_1 = v_{AVB} - v_{AVA}$

Mode 2
$$\dot{t} = 1$$
$$\dot{v}_i = I_i^s + f_{v_i}$$
$$\dot{v}_j = f_{v_j}$$
$$\dot{\sigma}_1 = 0$$
$$\dot{\sigma}_2 = 0$$
$$\tau \le \tau_f$$

$\tau \ge \tau_f$

$\sigma_2 = v_{AVB} - v_{AVA}$

Mode 3
$$\dot{t} = 1$$
$$\dot{v}_i = f_{v_i}$$
$$\dot{v}_j = f_{v_j}$$
$$\dot{\sigma}_1 = 0$$
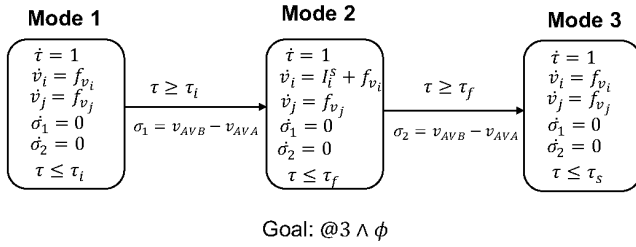$$\dot{\sigma}_2 = 0$$
$$\tau \le \tau_s$$

Goal: @3 ∧ φ

Fig. 6: The 3-mode hybrid automaton M_ϕ for response ϕ of the TW circuit

Parameter Uncertainty

C. elegans nervous system has been used for the study of fundamental problems in the function of neurons and neuronal circuits for many years. Due to its small size, the technique to record electrophysiological data, however, was simply not developed during the time when Wicks et al. derived the mathematical model for the TW circuit.

For this model, Wicks et al. extrapolated the electro-physiological data from Ascaris, a larger nematode related to C. elegans. Based on [25], they first assumed a standard membrane properties of each neuron in the TW circuit, such as, membrane capacitance, resistance etc., for a unit area. They then estimated the area based on the process lengths and cell diameter, measured using electron micrographs and branching morphology [26], [2], [27].

However, the diameter of the cell varies from 0.2 to 1.0 μm and the soma diameters of the process lengths, assuming the worm length of 1 mm, vary between 2 to 10 μm [27]. As a result, the surface area greatly varies, which, in turns, causes variability in membrane properties. Like the membrane

properties, the gap-junction and synaptic conductance varied among the population of the worms [28]. Both variability causes parameter uncertainty in the mathematical model of the TW circuit.

Estimating probability of each TW response on sReach:

Due to parameter uncertainty, we consider each parameter p of the Wicks et al. model as a random variable. As a result, M_ϕ becomes a stochastic hybrid automaton. Now for each response ϕ, we formulate a probabilistic reachability problem as follows:

Estimate the probability such that
$$\text{``Mode 3''} \land \phi \text{ is reachable in } M_\phi \quad (7)$$

We solve this problem on SReach.

V. RESULTS AND DISCUSSION

In this section, we solve problem 7 to estimate the probability of TW response patterns in various ablation groups. In our analysis, we consider each parameter as a random variable with both uniform and normal distribution.

As we discussed in Section IV, the values of the parameters are determined based on the size of surface area of neurons, gap-junctions and synapses. But these surface areas vary among population. According to [28], the area of gap-junction vary between 1 to 10 ncm^2 and standard gap-junction conductance per unit area (1 cm^2) is 1 S (Siemens) [29]. We use this information as the basis to consider 1 to 10 nS as the biologically relevant range for gap-junction conductance and g_i^{gap} is chosen by dividing capacitance of the corresponding neuron. However, as we could not find any biologically relevant ranges for synaptic and leakage conductance from the literature, we considered those parameters as constants according to the Table 1 from [11].

We performed our analysis on the control and five ablation groups. In each analysis, we consider Bayesian sequential estimation with 0.05 as the estimation error bound, 0.95 as the coverage probability, and a uniform prior ($\alpha = \beta = 1$). For initial condition, we first simulated the Wicks et al. model without applying any stimulation and then considered the steady state values from simulation as the initial conditions. We set the initial value of σ_1 and σ_2 to zero, stimulus current as 100 pA/pF and ϵ to 10^{-4} (0.1 mV). For computation, we used parallel version of SReach on a 32-core machine.

Table 1 shows the estimated probability of each TW response for all six groups, where we considered g_i^{gap} as a uniform random variable in the given range described above. In contrast, Table 2 shows the results where we considered them as a normal random variables. For the random distribution, we considered the values of g_i^{gap} chosen by Wicks et al. in [11] as mean. We, however, chose the variance in such a way so that the normal distribution cover 99% of the range of g_i^{gap}. In all cases, the predominant response in each group is highlighted in bold on both tables.

The predominant responses that we determined from our analysis for the four groups conform with the predominant

175

Group	REV		NR		F-ACC		F-DEC		FWD		B-ACC		B-DEC	
	Pr	RT (s)	Pr	RT (s)	Pr	RT (s)	Pr	RT (s)	Pr	RT (s)	Pr	RT (s)	Pr	RT (s)
Control	**0.83**	2343.87	0.039	252.58	0.015	26.37	0.121	897.47	0.015	26.37	0.015	26.37	0.015	26.37
PLM	**0.83**	1309.73	0.015	11.33	0.015	11.33	0.127	862.53	0.015	11.33	0.015	11.33	0.015	11.33
ALM-AVM	0.015	9.57	0.015	9.57	**0.689**	1578.83	0.33	1442.56	0.015	9.57	0.015	9.57	0.015	9.57
ALM-DVA	**0.414**	1406.31	0.0303	41.04	0.015	15.70	0.547	1766.48	0.015	15.70	0.015	15.70	0.015	15.70
AVM-PVC	0.015	3.33	0.015	3.33	0.015	3.33	0.015	3.33	0.015	3.33	**0.984**	255.21	0.015	3.33
AVM-PLM	0.03	72.02	0.015	16.49	0.015	16.49	**0.97**	419.39	0.015	16.49	0.015	16.49	0.015	16.49

TABLE I: Estimated probability and runtime for all response patterns by considering all g_i^{gap} as uniform random variables

responses that Wicks et al. obtained based on their ablation experiments on actual worm in [10]. Note that Wicks et al. did not differentiate the acceleration and deceleration responses in both forward and backward directions. As a result, their distributions on the TW responses have only three responses, as opposed to the seven responses in our distributions. In addition to these four groups, we performed analysis on two new ablation groups: AVM,PLM- and AVM,PVC-.

By comparing Table 1 with Table 2, we notice that the estimated probability of predominant response, computed by considering the parameters as normal random variables, is closer to the value obtained by Wicks et al. This indicates that the parameters are more likely to follow normal distribution over uniform distribution.

VI. RELATED WORK

Iyengar et al. [30] present a Pathway Logic (PL) model of neural circuits in the marine mollusk *Aplysia*. Specifically, the circuits they focus on are those involved in neural plasticity and memory formation. PL systems do not use differential equations, favoring qualitative symbolic models. They do not argue that they can replace traditional ODE systems, but rather that their qualitative insights can support the quantitative analysis of such systems. Neurons are expressed in terms of rewrite rules and data types.

Their simulations, unlike our reachability analysis, do not provide exhaustive exploration of the state space. Additionally, PL models are abstractions usually made in collaboration between computer scientists and biologists. Our work meets the biologists on their own terms, using the pre-existing ODE systems developed from physiological experiments.

Tiwari and Talcott [31] build a discrete symbolic model of the neural circuit Central Pattern Generator (CPG) in *Aplysia*. The CPG governs rhythmic foregut motion as the mollusk feeds. Working from a physiological (non-linear ODE) model, they abstract to a discrete system and use the Symbolic Analysis Laboratory (SAL) model checker to verify various properties of this system. They cite the complexity of the original model and the difficulty of parameter estimation as motivation for their abstraction.

In [12], we performed reachability analysis based on automatically computing discrepancy functions [13] on the Wicks et al. model [11] to estimate key model parameters for various TW responses. The technique, however, was not scalable enough to explore the entire parameter space of the model. In this work, on the other hand, we apply probabilistic reachability analysis to explore the large parameter space using SReach. Compared to methods that explore the entire sample spaces of random variables, such as ProbReach [32], SReach can handle complex systems with multiple random variables with affordable performance and without sacrificing the estimation accuracy. SReach has been successfully applied to real-world biological models - an atrial fibrillation model, a prostate cancer treatment model, and synthesized bacteria-killing procedure model - and cyber-physical systems [14].

VII. CONCLUSIONS

We present a probabilistic reachability analysis of the Wicks et al. model of the TW circuit in (C. elegans). In particular, we perform bounded-time probabilistic reachability analysis on this model to estimate the probability of various TW responses. The Wicks et al. model has a number of parameters, and we demonstrate that the various TW responses and their probability of occurrence in a population of worms can be viewed as a problem of *parameter uncertainty*.

Our approach to this problem rests on encoding each TW response as a hybrid automaton with parametric uncertainty. We then perform probabilistic reachability analysis on these automata using a technique that combines a δ-decision procedure with statistical tests. The results we obtain are a significant extension of those of Wicks et al., who equip their model with fixed parameter values that reproduce a single TW response. In contrast, our technique allow us to more thoroughly explore the models parameter space using statistical sampling theory, identifying in the process the distribution of TW responses. We show that our technique can be used to correctly estimate TW response-probabilities for the control group as well as three of ablation groups that Wicks et al. considered in wet-lab experiments. We also use our technique to *predict* TW response behavior for two ablation groups not previously considered by Wicks et al.

For future work, we intend to conduct ablation experiments to validate the results we obtained using our technique for two new groups. Furthermore, we will employ our probabilistic approach in order to define the parameter-space of a more detailed conductance-based model of C. elegans neurons where the calcium channels and pumps in each neuron are precisely modeled; consequently, one can compare the state of the art Ca^{2+} imaging data with our results.

Group	REV		NR		F-ACC		F-DEC		FWD		B-ACC		B-DEC	
	Pr	RT (s)	Pr	RT (s)	Pr	RT (s)	Pr	RT (s)	Pr	RT (s)	Pr	RT (s)	Pr	RT (s)
Control	**0.95**	801.78	0.030	87.45	0.015	16.48	0.038	282.67	0.015	16.48	0.015	16.48	0.015	16.48
PLM	**0.95**	639.06	0.015	10.49	0.015	10.49	0.04	164.72	0.015	10.48	0.015	10.48	0.015	10.48
ALM-AVM	0.015	8.57	0.015	8.57	**0.861**	973.60	0.158	728.97	0.015	8.57	0.015	8.57	0.015	8.57
ALM-DVA	**0.433**	1399.37	0.062	286.47	0.015	15.325	0.585	1518.54	0.015	16.48	0.015	16.48	0.015	16.48
AVM-PVC	0.015	3.33	0.015	3.33	0.015	3.33	0.015	3.33	0.015	3.33	**0.984**	255.21	0.015	3.33
AVM-PLM	0.015	19.27	0.015	19.27	0.015	19.27	**0.984**	458.66	0.015	19.27	0.015	19.27	0.015	19.27

TABLE II: Estimated probability and runtime for all response patterns by considering all g_i^{gap} as normal random variables

REFERENCES

[1] S. Brenner, "The genetics of caenorhabditis elegans," *Genetics*, vol. 77, no. 1, pp. 71–94, 1974.

[2] J. G. White, E. Southgate, J. N. Thomson, and S. Brenner, "The structure of the nervous system of the nematode caenorhabditis elegans," *Philos Trans R Soc Lond B Biol Sci*, vol. 314, no. 1165, pp. 1–340, 1986.

[3] E. L. Ardiel and C. H. Rankin, "An elegant mind: learning and memory in caenorhabditis elegans," *Learning & Memory*, vol. 17, no. 4, pp. 191–201, 2010.

[4] S. Kato, H. S. Kaplan, T. Schrödel, S. Skora, T. H. Lindsay, E. Yemini, S. Lockery, and M. Zimmer, "Global brain dynamics embed the motor command sequence of caenorhabditis elegans," *Cell*, vol. 163, no. 3, pp. 656–669, 2015.

[5] M. Zhen and A. D. Samuel, "C. elegans locomotion: small circuits, complex functions," *Current opinion in neurobiology*, vol. 33, pp. 117–126, 2015.

[6] M. B. Goodman, D. H. Hall, L. Avery, and S. R. Lockery, "Active currents regulate sensitivity and dynamic range in c. elegans neurons," *Neuron*, vol. 20, no. 4, pp. 763–772, 1998.

[7] E. R. Kandel and J. H. Schwartz, "Molecular biology of learning: modulation of transmitter release," *Science*, vol. 218, no. 4571, pp. 433–443, 1982.

[8] J. K. Rose and C. H. Rankin, "Analyses of habituation in caenorhabditis elegans," *Learning & Memory*, vol. 8, no. 2, pp. 63–69, 2001.

[9] C. I. Bargmann and L. Avery, "Laser killing of cells in caenorhabditis elegans," *Methods in cell biology*, vol. 48, pp. 225–250, 1995.

[10] S. R. Wicks and C. H. Rankin, "Integration of mechanosensory stimuli in Caenorhabditis Elegans," *The Journal of Neuroscience*, vol. 15, no. 3, pp. 2434–2444, 1995.

[11] S. R. Wicks, C. J. Roehrig, and C. H. Rankin, "A dynamic network simulation of the nematode tap withdrawal circuit: Predictions concerning synaptic function using behavioral criteria," *The Journal of Neuroscience*, vol. 16, no. 12, pp. 4017–4031, 1996.

[12] M. A. Islam, R. DeFrancisco, C. Fan, R. Grosu, S. Mitra, and S. A. Smolka, "Model checking tap withdrawal in C. Elegans," in *Hybrid Systems Biology*, pp. 195–210, Springer, 2015.

[13] C. Fan and S. Mitra, "Bounded verification with on-the-fly discrepancy computation," in *Automated Technology for Verification and Analysis*, pp. 446–463, Springer, 2015.

[14] Q. Wang, P. Zuliani, S. Kong, S. Gao, and E. M. Clarke, "Sreach: A probabilistic bounded delta-reachability analyzer for stochastic hybrid systems," in *International Conference on Computational Methods in Systems Biology*, pp. 15–27, Springer, 2015.

[15] N. Bhatla, "Wormweb." http://wormweb.org/.

[16] C. Koch and I. Segev, *Methods in neuronal modeling: from ions to networks*. MIT press, 1998.

[17] E. R. Kandel, J. H. Schwartz, T. M. Jessell, S. A. Siegelbaum, and A. Hudspeth, *Principles of neural science*, vol. 4. McGraw-hill New York, 2000.

[18] A. L. Hodgkin and A. F. Huxley, "A quantitative description of membrane current and its application to conduction and excitation in nerve," *The Journal of physiology*, vol. 117, no. 4, p. 500, 1952.

[19] T. Kawano, M. D. Po, S. Gao, G. Leung, W. S. Ryu, and M. Zhen, "An imbalancing act: gap junctions reduce the backward motor circuit activity to bias c. elegans for forward locomotion," *Neuron*, vol. 72, no. 4, pp. 572–586, 2011.

[20] J. M. Gray, J. J. Hill, and C. I. Bargmann, "A circuit for navigation in caenorhabditis elegans," *Proceedings of the National Academy of Sciences of the United States of America*, vol. 102, no. 9, pp. 3184–3191, 2005.

[21] J. T. Pierce-Shimomura, T. M. Morse, and S. R. Lockery, "The fundamental role of pirouettes in caenorhabditis elegans chemotaxis," *The journal of neuroscience*, vol. 19, no. 21, pp. 9557–9569, 1999.

[22] S. Gao, S. Kong, W. Chen, and E. M. Clarke, "δ-complete analysis for bounded reachability of hybrid systems," *CoRR*, vol. arXiv:1404.7171, 2014.

[23] S. Kong, S. Gao, W. Chen, and E. M. Clarke, "dReach: δ-reachability analysis for hybrid systems," in *Tools and Algorithms for the Construction and Analysis of Systems - 21st International Conference, TACAS, London, UK, April 11-18, 2015. Proceedings*, pp. 200–205, 2015.

[24] F. H. Fenton and E. M. Cherry, "Models of cardiac cell," vol. 3, no. 8, p. 1868, 2008. revision: 91508.

[25] W. Rall, "Cable theory for dendritic neurons," in *Methods in neuronal modeling*, pp. 9–92, MIT press, 1989.

[26] J. G. White, E. Southgate, J. N. Thomson, and S. Brenner, "The structure of the ventral nerve cord of caenorhabditis elegans," *Philosophical Transactions of the Royal Society B: Biological Sciences*, vol. 275, no. 938, pp. 327–348, 1976.

[27] W. B. Wood *et al.*, *The nematode Caenorhabditis elegans*. Cold Spring Harbour Laboratory, 1987.

[28] E. Niebur and P. Erdös, "Theory of the locomotion of nematodes: dynamics of undulatory progression on a surface," *Biophysical journal*, vol. 60, no. 5, p. 1132, 1991.

[29] M. Bennett, "A comparison of electrically and chemically mediated transmission," in *Structure and function of synapses*, pp. 221–256, Raven Press New York, 1972.

[30] S. M. Iyengar, C. Talcott, R. Mozzachiodi, E. Cataldo, and D. A. Baxter, "Executable symbolic models of neural processes,"

[31] A. Tiwari and C. L. Talcott, "Analyzing a discrete model of Aplysia central pattern generator," in *Proceedings of the 6th Conference on Computational Methods in Systems Biology (CMSB)*, pp. 347–366, Springer, 2008.

[32] F. Shmarov and P. Zuliani, "Probreach: verified probabilistic delta-reachability for stochastic hybrid systems," in *Proceedings of the 18th International Conference on Hybrid Systems: Computation and Control*, pp. 134–139, ACM, 2015.